ACS OMEGA

http://pubs.acs.org/journal/acsodf

Article

Thiophene-Derived Schiff Base Complexes: Synthesis, Characterization, Antimicrobial Properties, and Molecular Docking

Saira Nayab,* Aftab Alam, Nasir Ahmad, Sher Wali Khan, Waliullah Khan, Dilawar Farhan Shams, Muhammad Ishaq Ali Shah, Muhammad Ateeq, Said Karim Shah, and Hyosun Lee*

Cite This: *ACS Omega* 2023, 8, 17620−17633

Read Online

ACCESS | Metrics & More | Article Recommendations | Supporting Information

ABSTRACT: Novel thiophene-derived Schiff base ligand **DE**, where **DE** is (*E*)-N^1,N^1-diethyl-N^2-(thiophen-2-ylmethylene)-ethane-1,2-diamine, and the corresponding M(II) complexes, $[\mathbf{M(DE)X_2}]$ (M = Cu or Zn, X = Cl; M = Cd, X = Br), were prepared and structurally characterized. X-ray diffraction studies revealed that the geometry around the center of the M(II) complexes, $[\mathbf{Zn(DE)Cl_2}]$ and $[\mathbf{Cd(DE)Br_2}]$, could be best described as a distorted tetrahedral. *In vitro* antimicrobial screening of **DE** and its corresponding M(II) complexes, $[\mathbf{M(DE)X_2}]$, was performed. The complexes were more potent and showed higher activities against *Escherichia coli*, *Staphylococcus aureus*, and *Pseudomonas aeruginosa*, fungi *Candida albicans*, and protozoa *Leishmania major* compared to the ligand. Among the studied complexes, $[\mathbf{Cd(DE)Br_2}]$ exhibited the most promising antimicrobial activity against all the tested microbes compared to its analogs. These results were further supported by molecular docking studies. We believe that these complexes may significantly contribute to the efficient designing of metal-derived agents to treat microbial infections.

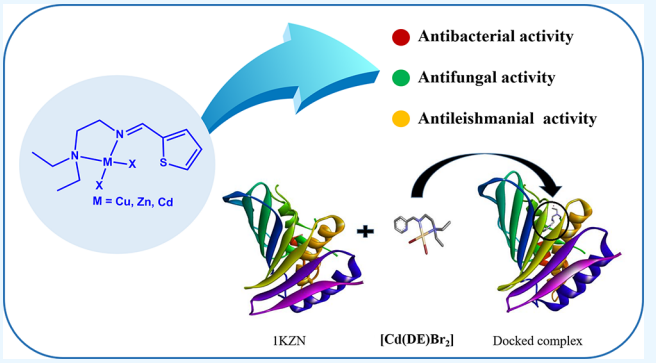

1. INTRODUCTION

In recent decades, the emergence of microbial resistance to antibiotics has been recognized as one of the biggest threats to global health.[1] Intensive research efforts are underway to highlight effective and innovative metal-derived active agents as potent antimicrobial drugs.[2] Metals alter the thermodynamic and kinetic properties of the complexes toward biological receptors owing to a broad range of oxidation states, nuclearities, and ligand architehtures.[3] Metal complexes may employ their effects by interacting with intracellular biomolecules, inhibiting enzymes, enhancing the lipophilic character, and varying cell membrane functions.[4]

Among the various ligands, nitrogen-containing ligands and their metal complexes have been explored as viable compounds for therapeutic and pharmacological purposes.[5] In particular, Schiff bases exhibit efficient bioactivity in a wide range of biological applications.[6] Much attention has been given to ligands derived from Schiff base owing to their exceptional structural and synthetic flexibility, fine tunability, and selectivity toward the transition metal atom[1,6,7] to form *N*,*N*′-bidentate,[8] *N*,*N*′,X-tridentate, and *N*,*N*′,*N*″,X-tetradentate[9] geometries. Schiff bases regulate the performance of metals in a wide array of useful catalytic transformations, such as catalytic activity in the hydrogenation of olefins, ring-opening polymerization (ROP) of cyclic olefins, and pharmacological and biological applications.[10] Metal complexes with Schiff base scaffolds comprising heterocyclic moieties have gained notable attention as broad-spectrum antimicrobial agents.[11]

Recently, thiophene[12]-derived Schiff base ligands have become increasingly popular owing to their biological significance. For instance, morpholine-(iso)thiosemicarbazone Cu(II) complexes exhibit promising anticancer potential against human ovarian cancer and antibacterial potential against *Staphylococcus aureus* (*S. aureus*) with MIC_{50} values of 2−5 $\mu g\ mL^{-1}$.[13] Moinuddin et al. recently studied *N*′-(3-hydroxybenzoyl)thiophene-2-carbohydrazide-based Co(II) and Cu(II) complexes, which exhibited remarkable cytotoxicity in MCF-7 and HeLa cell lines and also had the antifungal and antioxidant potential.[11e] Similarly, 2-aminomethylthiophenyl-4-bromosalicylaldehyde-based Zn(II) complexes displayed MIC values in the 0.06−9.9 $\mu g\ mL^{-1}$ range for studied bacterial species and in the 1.95−7.81 $\mu g\ mL^{-1}$ range for studied fungal species.[14] Chohan et al. studied Ni(II), Co(II), and Cu(II) complexes supported with thiophene-based diamines, which exhibited promising antibacterial/antifungal potential against six

Received: December 30, 2022
Accepted: April 19, 2023
Published: May 12, 2023

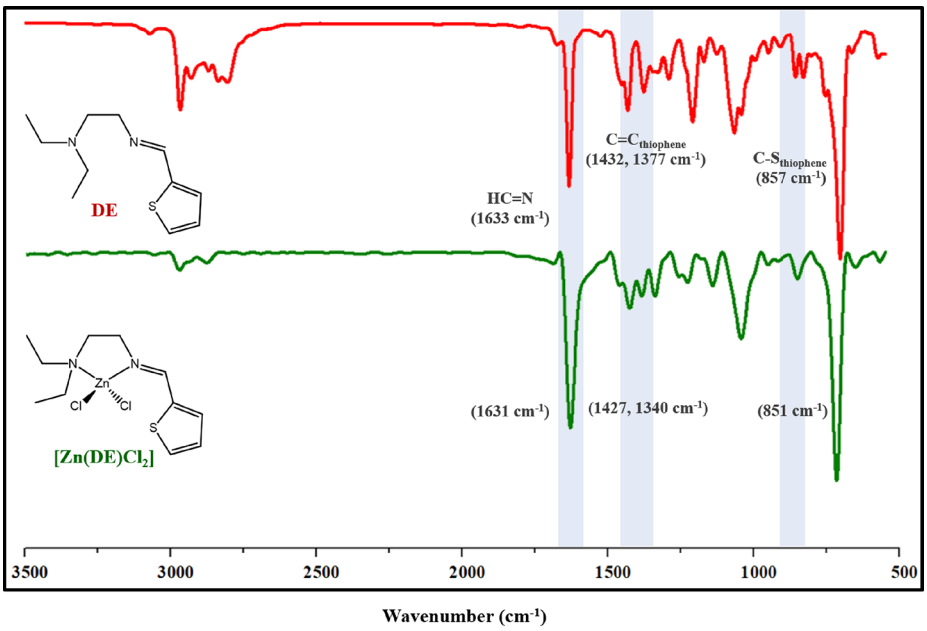

Figure 1. FTIR spectrum of **DE** (top) and $[\mathbf{Zn(DE)Cl_2}]$ (bottom).

fungal and bacterial strains.[12b] There is a dire need for the development of novel and potent antimicrobial agents with improved pharmacodynamic and pharmacokinetic characteristics.[15] The significance of thiophene-derived compounds, with their wide range of biological properties, prompted us to design new thiophene-derived C_1-symmetric Schiff base ligand **DE** and its transition metal complexes to be used as antimicrobial agents. $[\mathbf{M(DE)X_2}]$ complexes were synthesized and investigated for their bactericidal, fungicidal, and leishmanicidal potential.

2. MATERIALS AND METHODS

2.1. Materials. All manipulations involved in the synthesis of the ligand (**DE**), and the corresponding M(II) complexes, $[\mathbf{M(DE)X_2}]$, were accomplished using benchtop techniques unless specified. Reagents, including thiophene-2-carbaldehyde, N^1,N^1-diethylethane-1,2-diamine, copper chloride dihydrate ($CuCl_2{\cdot}2H_2O$), cadmium bromide tetrahydrate ($CdBr_2{\cdot}4H_2O$), zinc dichloride ($ZnCl_2$), and drying agent magnesium sulfate ($MgSO_4$), were purchased from Sigma-Aldrich Corp. Solvents used in synthesis such as methanol (MeOH), *n*-hexane (*n*-hex), dichloromethane (CH_2Cl_2), diethyl ether (Et_2O), ethanol (EtOH), ethyl acetate (EtOAc), and dimethyl sulfoxide (DMSO) were obtained from Merck and used as received. The reagents for antimicrobial activities were purchased from Sigma-Aldrich and used as received.

2.2. Instrumentation. Melting points of $[\mathbf{M(DE)X_2}]$ complexes were determined using an IA9100 Electrothermal apparatus. The NMR spectrum was recorded on a Bruker Avance III spectrometer (500 MHz for ^{1}H NMR and 125 MHz for ^{13}C NMR) (Figures S1−S6). Tetramethylsilane (TMS) was used as an internal standard, and chemical shifts are recorded in ppm units (δ); coupling constants (J) are reported in Hertz (Hz). The FTIR spectra of **DE** and its corresponding $[\mathbf{M(DE)X_2}]$ complexes were recorded on a Bruker FT/IR-Alpha (neat; cm^{-1}) (Figure 1 and Figures S7 and S8). Elemental analysis of complexes, $[\mathbf{M(DE)X_2}]$, was achieved using an EA-1108 Carlo-Erba elemental analyzer (Figure S9). Molar conductance (Ω^{-1} cm^2 mol^{-1}) in DMSO (1×10^{-5} M at room temperature) solution was determined using a Digital Multi-meter 73301. The electronic absorption spectra of the ligand and corresponding M(II) complexes in the DMSO solution (1×10^{-3} M) were recorded using a Cary-50 UV−Visible spectrophotometer. Thermogravimetric analysis was performed on a thermal analyzer (TGA-Q500) with mass loss measurement from 25 to 900 °C under a N_2 atmosphere at a heating rate of 10 °C min^{-1}.

2.3. Synthesis. *2.3.1. N^1,N^1-Diethyl-N^2-(thiophen-2-ylmethylene)ethane-1,2-diamine (**DE**).* A CH_2Cl_2 solution of 2-thiophenecarbaldehyde (2.77 g, 24.75 mmol) was added to a CH_2Cl_2 solution of N^1,N^1-diethylethane-1,2-diamine (3.00 g, 24.75 mmol) and stirred at 25 °C for 48 h. TLC was used to check the progress of the reaction (*n*-hex:EtOAc, 2:8 as a developing solvent). The reaction mixture was washed with aqueous NaCl solution (10.0 mL × 2), and the separated organic layer was treated with $MgSO_4$ as a drying agent and filtered. The solution was concentrated to furnish a light brown oil liquid. Vacuum distillation was carried out to get the final product as a lemon color oil (3.50 g, 93%). ^{1}H NMR (500 MHz, $CDCl_3$, ppm): δ = 8.38 (1H, s, N=C***H***), 7.38 (1H, td, J = 4.29 Hz, 1.34 Hz, Ar-***H***), 7.29 (1H, dd, J = 4.44 Hz, 2.96 Hz, Ar-***H***), 7.06 (1H, m, Ar-***H***), 3.68 (2H, m, (=N-C***H***$_2$)), 2.76 (2H, m, $(CH_3-CH_2)_2$-N-C***H***$_2$), 2.59 (4H, q, J = 7.31 Hz, $(CH_3-C\mathbf{H}_2)_2$-N), 1.04 (6H, t, J = 7.31 Hz, $(C\mathbf{H}_3-CH_2)_2$-N). ^{13}C NMR (125 MHz, $CDCl_3$, ppm): δ = 154.7 (-N=**C**H-), 142.48 (Ar-**C**), 130.0 (Ar-**C**), 128.5 (Ar-**C**), 127.1 (Ar-**C**), 59.4 (=N-**C**H$_2$), 53.3 (**C**H$_2$-N-CH$_2$-CH$_3$), 47.4 (CH$_2$-N-(**C**H$_2$-CH$_3$)$_2$), 11.9 (CH$_2$-N-(CH$_2$-**C**H$_3$)$_2$). UV−Vis (DMSO; 1×10^{-3} M): 283 (n → π^*); 268 ($\pi \rightarrow \pi^*$). FTIR (cm^{-1}): ν(C−H; sp^2) 2967 w; ν(C−H; sp^3) 2930 w; ν(C=N) 1633 s; $\nu(C=C)_{thiophene}$ 1432 m; δ(C−H; sp^3) 1329 w; ν(C−N) 1027 s; ν(C−S) 857 w.

*2.3.2. (E)-N^1,N^1-Diethyl-N^2-(thiophen-2-ylmethylene)-ethane-1,2-diamine Dichloro Cu(II) Complex, **[Cu(DE)Cl$_2$]**.* An EtOH solution of **DE** (1.00 g, 4.60 mmol) was added dropwise to an EtOH solution of $CuCl_2$ (1.06 g, 4.60 mmol) at room temperature. A green precipitate appeared while stirring at 25 °C for 2 h. The precipitate was filtered and washed with cold EtOH (10.0 mL × 2) and Et_2O (10.0 mL × 2) to yield the final product (1.50 g, 88%). MP (°C): 150. Elemental analysis:

https://doi.org/10.1021/acsomega.2c08266
ACS Omega 2023, 8, 17620−17633

$C_{11}H_{18}Cl_2CuN_2S$ (%): C, 38.32; H, 5.26; N, 8.12; Found: C, 38.39; H, 5.43; N, 8.45. UV−Vis (DMSO; 1×10^{-3} M): 281 (n → π*); 265 (π → π*). FTIR (cm^{-1}): ν(C−H; sp^2) 2951 w; ν(C−H; sp^3) 2867 w; ν(C=N) 1633 s; $\nu(C=C)_{thiophene}$ 1463 m, 1386 m; δ(C−H; sp^3) 1387 w; ν(C−N) 1217 s; ν(C−S) 805 w.; ν(M−N) 572 w. Molar conductivity in DMSO (1.0×10^{-5} M; Ω^{-1} cm^2 mol^{-1}): 13.

2.3.3. (E)-N¹,N¹-Diethyl-N²-(thiophen-2-ylmethylene)-ethane-1,2-diamine Dichloro Zn(II) Complex, [Zn(DE)Cl₂]. [**Zn(DE)Cl₂**] was synthesized according to the similar procedure described for [**Cu(DE)Cl₂**] except utilizing an EtOH solution of $ZnCl_2$ (0.627 g, 4.60 mmol) to get a white crystalline solid as the final product (1.50 g, 92%). Single crystals of [**Zn(DE)Cl₂**] suitable for X-ray diffraction analysis were obtained by layering *n*-hex on the CH_2Cl_2 solution of [**Zn(DE)Cl₂**]. MP (°C): 183. Elemental analysis: $C_{11}H_{18}Cl_2N_2SZn$ (%): C, 38.12; N, 8.08; H, 5.23. Found: C 38.28; N 8.00; H 5.24. ^{1}H NMR (500 MHz, $CDCl_3$, ppm): δ = 8.54 (1H, s, N=C***H***), 7.91 (1H, m, Ar-***H***), 7.78 (1H, d, *J* = 4.98 Hz, Ar-***H***), 7.21 (1H, m, Ar-***H***), 3.85 (2H, m, CH_3-CH_2)$_2$-N-C***H***$_2$), 3.25 (2H, sextet, *J* = 14.09 Hz, 7.31 Hz, (CH_3-C***H***$_2$)$_2$-N), 3.03 (2H, t, *J* = 6.59 Hz, (CH_3-CH_2)$_2$-N-C***H***$_2$) 2.92 (2H, sextet, *J* = 14.09 Hz, 8.05 Hz, (CH_3-C***H***$_2$)$_2$-N), 1.21 (6H, t, *J* = 7.34 Hz, (C***H***$_3$-CH_2)$_2$-N). ^{13}C NMR (125 MHz, $CDCl_3$, ppm): δ = 162.0 (-N=***C***H-), 136.8 (Ar-***C***), 135.5 (Ar-***C***), 128.7 (Ar-***C***), 128.5 (Ar-***C***), 59.1 (=N-***C***H$_2$), 52.1 (***C***H$_2$-N-CH$_2$-CH$_3$), 44.5 (CH$_2$-N-(***C***H$_2$-CH$_3$)$_2$), 8.26 (CH$_2$-N-(CH$_2$-***C***H$_3$)$_2$). UV−Vis (DMSO; 1×10^{-3} M): 280 (n → π*); 263 (π → π*). FTIR (cm^{-1}): ν(C−H; sp^2) 2974 w; ν(C−H; sp^3) 2876 w; ν(C=N) 1631 s; $\nu(C=C)_{thiophene}$ 1427 m, 1340 m; δ(C−H; sp^3) 1341 w; ν(C−N) 1226 s; ν(C−S) 851 w; ν(M−N) 566 w. Molar conductivity in DMSO (1.0×10^{-5} M; Ω^{-1} cm^2 mol^{-1}): 11.

2.3.4. (E)-N¹,N¹-Diethyl-N²-(thiophen-2-ylmethylene)-ethane-1,2-diamine Dichloro Cd(II) Complex, [Cd(DE)Br₂]. [**Cd(DE)Br₂**] was synthesized according to the similar procedure described for [**Zn(DE)Cl₂**] except utilizing $CdBr_2 \cdot 4H_2O$ (1.06 g, 4.60 mmol) to yield a white solid as the final product (1.53 g, 90%). MP (°C): 151. [**Cd(DE)Br₂**] suitable for X-ray diffraction analysis were obtained by layering *n*-hex on the CH_2Cl_2 solution of [**Cd(DE)Br₂**]. Elemental analysis: $C_{11}H_{18}Br_2CdN_2S$ (%): C, 27.38; H, 3.76; N, 5.81: Found C, 27.51; H, 3.71; N, 5.86. ^{1}H NMR (500 MHz, $CDCl_3$, ppm): δ = 8.61 (1H, s, N=C***H***-), 7.70 (1H, d, *J* = 4.79 Hz, Ar-***H***), 7.65 (1H, d, *J* = 3.65 Hz, Ar-***H***), 7.19 (1H, m, Ar-***H***), 3.85 (2H, m, (CH_3-CH_2)$_2$-N-C***H***$_2$), 3.18 (2H, m, (CH_3-C***H***$_2$)$_2$-N), 3.00 (2H, m, (CH_3-CH_2)$_2$-N-C***H***$_2$), 2.92 (2H, m, (CH_3-C***H***$_2$)$_2$-N), 1.21 (6H, t, *J* = 6.66 Hz, (C***H***$_3$-CH_2)$_2$-N). ^{13}C NMR (125 MHz, $CDCl_3$, ppm): δ = 161.6 (-N=***C***H-), 136.2 (Ar-***C***), 135.1 (Ar-***C***), 133.6 (Ar-***C***), 128.3 (Ar-***C***), 54.8 (=N-***C***H$_2$), 53.3 (***C***H$_2$-N-CH$_2$-CH$_3$), 45.3 (CH$_2$-N-(***C***H$_2$-CH$_3$)$_2$), 8.98 (CH$_2$-N-(CH$_2$-***C***H$_3$)$_2$). UV−Vis (DMSO; 1×10^{-3} M): 281 (n → π*); 264 (π → π*). FTIR (cm^{-1}): ν(C−H; sp^2) 2973; ν(C−H; sp^3) 2875; ν(C=N) 1627 s; $\nu(C=C)_{thiophene}$ 1430 m, 1388 m; δ(C−H; sp^3) 1347 w; ν(C−N) 1269 s; ν(C−S) 845 w; ν(M−N) 644 w. Molar conductivity in DMSO (1.0×10^{-5} M; Ω^{-1} cm^2 mol^{-1}):10.

2.4. X-ray Crystallography. The diffraction data of single crystals was recorded with synchrotron radiations (λ = 0.630 Å, at 293(2) K) using a Rayonix MX225HS-detector at 2D SMC with a silicon double crystal monochromator. For data collection, PAL BL2D-SMDC software[16] (with a detector distance of 63 mm, omega scan; Δω = 1° and exposure time of 1 s/frame) was used. For cell refinement and absorption correction, HKL3000sm (Ver. 703r)[17] was employed. APEX 4 Software was employed for collection of data, and the intensity data were corrected for absorption with the SADABS program (T_{min}/T_{max} = 0.874).[18] Solving of crystal structures was done by the intrinsic phasing method with SHELXT[19] and refined by full-matrix least-squares refinement using the SHELXL-2018/3 program.[20] Anisotropic displacement factors were employed for refinement of nonhydrogen atom positions. Hydrogen atom positions were constrained relative to their parent atoms using the appropriate HFIX command in SHELXL-2018/3.[20] Structural refinements and crystallographic data for [**Zn(DE)Cl₂**] and [**Cd(DE)Br₂**] are summarized in Table 1.

2.5. Antimicrobial Activity. *2.5.1. Antibacterial Assay.* The bactericidal properties of the newly synthesized ligand (**DE**) and complexes [**M(DE)X₂**] were evaluated using the agar standard diffusion procedure, in which the agar plate was swabbed with a standard concentration of the test organisms,

Table 1. Structure Refinements and Crystallographic Data of [Zn(DE)Cl₂] and [Cd(DE)Br₂]

	[Zn(DE)Cl₂]	[Cd(DE)Br₂]
empirical formula	$C_{11}H_{18}Cl_2N_2SZn$	$C_{11}H_{18}Br_2CdN_2S$
formula weight	346.60	482.55
temperature (K)	293(2)	293(2)
wavelength (Å)	0.630	0.630
crystal system	monoclinic	monoclinic
space group	$P2_1/n$	$P2_1/n$
unit cell dimensions		
a (Å)	6.9460(14)	10.069(2)
b (Å)	9.6140(19)	15.515(3)
c (Å)	22.239(4)	10.339(2)
β (°)	97.46(3)	98.28(3)
volume ($Å^3$)	1470.8(5)	1598.3(6)
Z	4	4
density (calculated) (mg/m^3)	1.564	2.005
absorption coefficient (mm^{-1})	1.539	4.700
F(000)	712	928
crystal size (mm^3)	0.100 × 0.050 × 0.040	0.078 × 0.050 × 0.045
θ range for data collection (°)	1.637 to 33.544	2.114 to 22.500
index ranges	$-11 \le h \le 11, -15 \le k \le 15, -33 \le l \le 33$	$-12 \le h \le 12, -18 \le k \le 18, -12 \le l \le 12$
reflections collected	21,390	10,207
independent reflections	6463 [R_{int} = 0.0460]	3005 [R_{int} = 0.0670]
completeness to θ = 22.210°	96.0%	100.0%
absorption correction	empirical	empirical
max. and min. transmission	1.000 and 0.941	1.000 and 0.853
refinement method	full-matrix least-squares on F^2	full-matrix least-squares on F^2
data/restraints/parameters	6463/0/156	3005/0/157
goodness-of-fit on F^2	1.189	1.143
final *R* indices [$I > 2\sigma(I)$]	R_1 = 0.0417, wR_2 = 0.1268	R_1 = 0.0372, wR_2 = 0.1138
R indices (all data)	R_1 = 0.0450, wR_2 = 0.1296	R_1 = 0.0375, wR_2 = 0.1142
largest diff. peak and hole (e.$Å^{-3}$)	1.147 and −1.386	2.089 and −1.701

https://doi.org/10.1021/acsomega.2c08266
ACS Omega 2023, 8, 17620−17633

Scheme 1. Schematic Illustration of the Preparation of DE and Corresponding M(II) Complexes

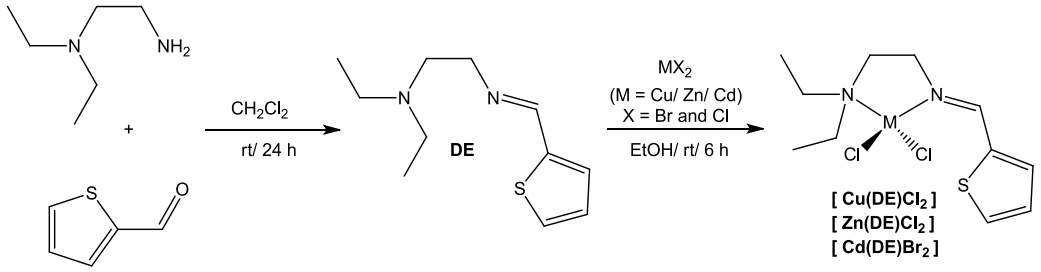

i.e., *E. coli*, *P. aeruginosa*, and *S. aureus*, followed by placing a paper disk containing specific concentrations of the test compound on bacterial culture.[21] The bacterial strains were tested against three different concentrations, i.e., 500, 250, and 100 μg mL^{-1}, of assessed compounds (dissolved in DMSO) using chloramphenicol as a standard drug with the same concentrations. The antimicrobial activity was assayed by measuring inhibition zone diameter (mm) formed around the well. Each compound was tested in triplicate, and the results were noted and inferred according to standards.

A broth macrodilution method evaluated the minimum inhibitory concentrations (MICs) against the bacteria (*E. coli*, *P. aeruginosa*, and *S. aureus*) of the test compounds. Mueller−Hinton Broth (MHB) was used as a medium. Small sterile tubes (1.00 mL) were used to perform this assay. Isolated tubes were used for the preparation of different concentrations of the test compounds. MHB medium (500 μL) was distributed into each glass tube. The bacterial strain and standardized bacterial suspension of 0.5 McFarland turbidity were added to tubes containing different concentrations of test compounds. A bacterium in an antibiotic-free medium and bacteria with antibiotics were also prepared. The tubes were later incubated for 24 h at 37 °C. The inhibition of the tested compound was recorded with the highest dilution having no turbidity. The tube with MIC at which no bacterial growth was observed was further diluted to record the optimum MICs of the compound.[22]

2.5.2. Antifungal Assay. For the screening of antifungal properties of compounds against *C. albicans*, the agar well diffusion technique[22] was employed with chloramphenicol as a positive control. First, Sabouraud dextrose agar (SDA) was prepared and autoclaved at 121 °C and transferred into Petri plates. To prepare a 0.5 McFarland standard, 0.05 L of 1.175% $BaCl_2{\cdot}2H_2O$ was mixed with 9.95 mL of 1% H_2SO_4. The 24 h culture of *C. albicans* inoculum was grown using the SDA. The cell suspension was prepared in a sterilized saline solution (0.85%). To attain the final concentration to that of 0.5 McFarland, the turbidity of fungal suspension was adjusted. A 0.5 McFarland standard inoculum was used to make the fungal cell lawn on SDA plates. In the Petri plates, 4 mm walls were made. The test compounds in various concentrations were added to the wells and incubated at 35 °C for 48 h.

2.5.3. Antileishmanial Assay. The antileishmanial activities of **DE** and its M(II) complexes, [**M(DE)X$_2$**], were determined using the previously developed method by Habtemariam..[23] Pre-established culture of *L. major* was inoculated in 199 media in Novy-MacNeal-Nicole-medium slants and incubated for 6−7 days at 24 °C. A stock solution (1000 μg mL^{-1}) was prepared by dissolving 1.00 mg of each test compound in 1.00 mL of DMSO followed by serial dilution of stock solution. A total of 180 μL of 199 medium was added in different 96-well microtiter plate wells. For each test compound, 20 μL was added to the first well and then serially diluted, and to keep the final volume of 180 μL, 20 μL was discarded from the last well. About 100 μL of the parasite was added to each well, and two rows were left for positive (amphotericin B) and negative control (DMSO). Microtiter plates were incubated for 24 °C for 72 h. A total of 20 μL was taken from each dilution after the incubation period, and live parasites were mounted under a microscope using an improved Neubauer counting chamber. The leishmanicidal assay was performed in triplicate. IC_{50} values of compounds possessing leishmanicidal potential were calculated by Prism software (GraphPad Software, San Diego, CA).

2.6. Molecular Docking. The PDB IDs of the crystal structure of *E. coli* (24 kDa) are actually a clorobiocin complex with 2.30 Å resolution, and DNA gyrase is involved in replication and transcription of major proteins. The bacterial DNA negative supercoiling is also catalyzed by DNA gyrase, and bacterial cell death is induced when it is targeted by external bacterial agents. 4CL6 is the crystal structure of the *P. aeruginosa* protein complex with a resolution of 2.41 Å. The biosynthetic pathway of fatty acid synthase (FAS) involved reduction, dehydration, and chain elongation reactions in both prokaryotes and eukaryotes, but the FAS pathway in eukaryotic cells is completely different from the FASII pathway in prokaryotic cells. The FASII enzyme is therefore targeted by bacterial agents against Gram-negative bacteria for antibiotic developments.

3FYV is the crystal structure of *S. aureus* DHFR protein complex with a resolution of 2.20 Å, which catalyzes the hydride transfer from NADPH to DHF.[24] The DHFR enzyme plays a key role in the THF pathway by maintaining a sufficient amount of cofactors involved in biosynthesis of purine nucleotides, methionine, thymidylate, and panthothenate.[25] The inhibition of DHFR enzyme results in stoppage of cell division and DNA synthesis, which lead to cell death, and thus, DHFR is the main target of different antibiotics in various parasitic and bacterial infections.[26] 5FSA is the crystal structure of the *C. albicans* protein complex with a resolution of 2.86 Å, which is required for sterol biosynthesis in eukaryotic cells and thus is the main target of therapeutic agents used for fungal treatments. Meanwhile, 2JK6 is the crystal structure of *Leishmania infantum* with a resolution of 2.95 Å,[27] which is involved in thiol-based metabolism[28] and thus is the main target of therapeutic agents used for Leishmania treatments.[29]

These structures were used for molecular docking as a receptor, and active sites were selected. The protein receptors were docked with four different compounds. The Molecular Operation Environment (MOE) 2014 program was used for docking.[30] The hybridization state assignment for each residue, charge corrections, missing hydrogen addition, and water molecule removal were done before docking. The GB/VI electrostatic function was used for protonation correction in different confirmations for each docking compound, and the

https://doi.org/10.1021/acsomega.2c08266
ACS Omega 2023, 8, 17620−17633

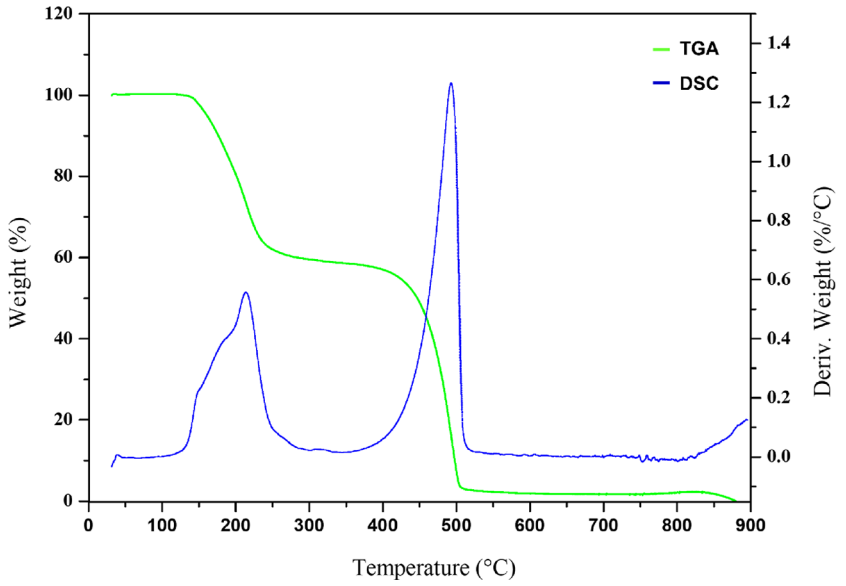

Figure 2. TGA-DTA thermogram of $[\mathbf{Cd(DE)Br_2}]$.

London docking scoring function was used for free energy calculation.[30] The binding affinities were calculated by the GBVI/WSA method, which represent the nonbonding interaction energy between the receptor and docking compound, and after energy minimization, the binding affinities were calculated.[31]

3. RESULTS AND DISCUSSION

3.1. Synthesis and Physical Properties. Schiff bases with O- and S-bearing heterocyclic rings show enhanced biological activities because of their similarities to natural products and synthetic compounds with promising activities.[32] In our study, the C_1-symmetric thiophene-derived Schiff base ligand (**DE**) was obtained as a yellow oil in a single step, as shown in Scheme 1. The condensation reaction of thiophene-2-carbaldehyde with N^1,N^1-diethylethane-1,2-diamine yielded an appreciable amount of ligand (93%). The obtained ligand was purified by vacuum distillation, and spectro-analytical techniques were used for structure elucidation.

Ligands with a nitrogen donor atom having different hybridizations are readily coordinated to the metal center. In this regard, metals easily accept the Schiff base ligand (**DE**) upon reacting with $CuCl_2{\cdot}2H_2O$, $ZnCl_2$, and $CdBr_2{\cdot}4H_2O$ to form monomeric complexes, $[\mathbf{M(DE)X_2}]$, in appreciable yields (88−92%). The $[\mathbf{M(DE)X_2}]$ (M = Zn or Cd; X = Cl or Br) complexes were obtained as white crystalline solids, whereas the Cu(II) complex was obtained as a blue-green solid. The complexes were purified *via* recrystallization from EtOH. The electronic spectra for the studied ligand and corresponding M(II) complexes were obtained in DMSO, and absorption bands at approximately 264−268 nm are ascribed to the $\pi \rightarrow \pi^*$ transitions existing in the aromatic ring.[33] Bands corresponding to $n \rightarrow \pi^*$ transition are observed at approximately 280 nm due to the characteristic HC═N group[33a] (Figure S10). The UV−visible spectra of $[\mathbf{M(DE)X_2}]$ complexes showed identical absorption spectra to **DE** with a slight shift in wavelength, signifying the ligation of the nitrogen atoms of **DE** to the metal centers.[33b,34] Additionally, a representative time-stability curve of $[\mathbf{Cd(DE)Br_2}]$ at 0 and 48 h is shown in Figure S11. There is no significant variation observed in the position and intensity of the absorption maxima of the studied complex during this period of time, signifying the solution stability of the studied complex.

The FTIR spectrum of **DE** exhibited a strong peak at 1633 cm^{-1} (Figure 1), characteristic of the C═N functional group.[34,35] Additionally, the absorption band characteristic of the υ(C═O) bond from thiophene-2-carboxaldehyde disappeared, demonstrating that the reaction was complete and confirming that the imine ligand was successfully synthesized. The representative $(C{=}N)_{imine}$ bond stretch appeared in the range of 1634−1627 cm^{-1} in $[\mathbf{M(DE)X_2}]$.[36] It was evident from the spectral data that the $(C{=}N)_{imine}$ bond shifted to higher wavenumbers (cm^{-1}) in the spectra of $[\mathbf{M(DE)X_2}]$ complexes, in comparison to the free ligand (**DE**), signifying the involvement of imine nitrogen in bonding.[37] The vibration peak found in the 1432−1377 cm^{-1} range was assigned to the symmetrical and asymmetrical υ(C═C) stretching vibrations of the thiophene ring, which shifted to the range of 1435−1384 cm^{-1} for the corresponding M(II) complexes. In addition, the (C−S−C) absorption band of the thiophene ring appeared at 857 cm^{-1}.[38] Typical peaks for the aromatic C═C, C−H bond stretching appeared at the expected ranges, as reported in the literature for similar complexes.[36] Notably, no bands were observed in the range of 421−418 cm^{-1} corresponding to the ν(M−S) stretching vibrations in the spectra of complexes, confirming that sulfur in thiophene had not participated in the complexation.[38]

The formation of the ligand was also confirmed by ^{1}H NMR spectroscopy; the disappearance of an aldehyde peak and the appearance of an imine proton peak at 8.38 ppm in the NMR spectrum of **DE** were evident (Figure S1).[35,37b] In addition, the protons of the ethylene backbone resonated at 3.68 and 2.76 ppm in **DE**. The structural characterization of Zn(II) and Cd(II) complexes *via* NMR spectroscopy revealed a slight shift of an imine proton from 8.38 to 8.54 ppm for $[\mathbf{Zn(DE)Cl_2}]$ and 8.61 ppm for $[\mathbf{Cd(DE)Br_2}]$. All the signals for carbon in the organic framework of the complexes were in agreement with the expected structures. The studied complexes were non-hygroscopic and stable toward atmospheric components. The complexes were soluble in CH_2Cl_2, THF, dimethylformamide, and DMSO but insoluble in Et_2O, *n*-hex, and water at room

https://doi.org/10.1021/acsomega.2c08266
ACS Omega 2023, 8, 17620−17633

temperature. The molar conductance values obtained at room temperature in DMSO for the studied complexes were low, which was indicative of the non-electrolytic nature of the $[M(DE)X_2]$ complexes. The conductivities of studied complexes remained constant even after 3 h, representing that no dissociation had occurred in the solution.[39] The purity of the complexes $[M(DE)X_2]$ was verified by percentage composition analysis of carbon, hydrogen, and nitrogen constituents, and good correlations were found between the calculated and experimental values (Figure S9).

The thermal stability profile of $[Cd(DE)Br_2]$ is presented in Figure 2. The TGA curve of $[Cd(DE)Br_2]$ demonstrated stability up to 140 °C and no loss in weight of complex occurred before this temperature region, which infers the absence of coordinated water molecules. The decomposition occurred in two steps; decomposition started with an exothermic DSC peak in the range of 140−240 °C. It is attributed to the loss of bromide ions and dissociation of the thiophene moiety, and this step brings a weight loss of 40%. The resultant residue of the complex underwent a second-stage degradation in the 375−510 °C range with a weight loss of 54% because of the decomposition of the ligand molecule. A horizontal thermal curve[40] was observed above 500 °C. The $[Zn(DE)Cl_2]$ profile represents stability up to 190 °C. The single-step decomposition started at 190 °C and ended at 480 °C, resulting in a horizontal thermal curve above 470 °C (Figure S12). In the case of the Cu(II) complex, $[Cu(DE)Cl_2]$, no weight loss has been observed up to 250 °C. The loss between 250 and 370 °C with an exothermic peak in the 250−350 °C range is associated with the loss of chloride ions and thiophene moiety. Second-stage degradation in the 500−700 °C range with a weight loss of 44% represents the decomposition of $[Cu(DE)Cl_2]$, which might be in the form of CuO above 700 °C. This step is also accompanied by exothermic peaks (Figure S13).[40]

3.2. Molecular Structures of Complexes. The precise structural properties of studied complexes were determined with X-ray diffraction studies. ORTEP drawings of $[Zn(DE)Cl_2]$ and $[Cd(DE)Br_2]$ are depicted in Figures 3 and 4, respectively.

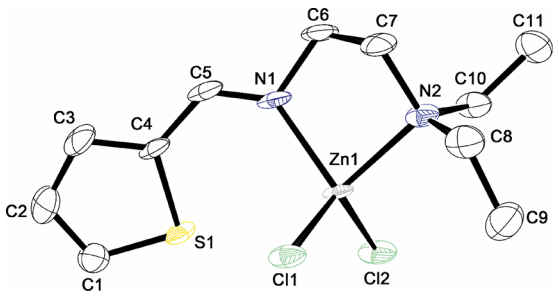

Figure 3. ORTEP drawing of $[Zn(DE)Cl_2]$ with thermal ellipsoids at 70% probability. All hydrogen atoms are omitted for clarity.

Selected bond lengths (Å) and angles (°) for these complexes are presented in Table 2. The geometry around the tetracoordinate Zn(II) and Cd(II) centers in $[Zn(DE)Cl_2]$ and $[Cd(DE)Br_2]$ can be described as a distorted tetrahedral attained *via* ligation with the nitrogen atoms of the azomethine and amine moieties of the **DE** ligand. Based on the τ_4 values, Zn(II) and Cd(II) complexes exhibited distorted tetrahedral geometries (Table 3).[41] Additionally, the THC_{DA} index[42] for differentiation of tetrahedral and trigonal pyramidal geometries (a perfect tetrahedral structure generates a THC_{DA} index = 100,

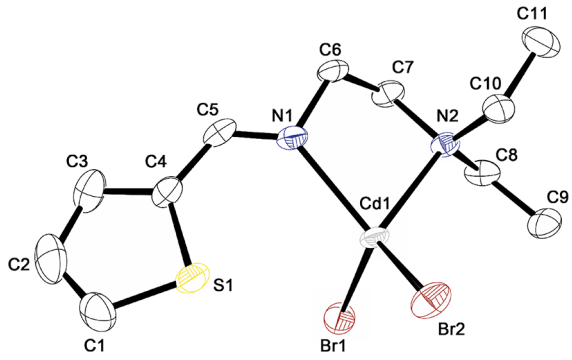

Figure 4. ORTEP drawing of $[Cd(DE)Br_2]$ with thermal ellipsoids at 50% probability. All hydrogen atoms are omitted for clarity.

Table 2. Selected Bond Distances (Å) and Angles (°) of $[Zn(DE)Cl_2]$ and $[Cd(DE)Br_2]$

$[Zn(DE)Cl_2]$		$[Cd(DE)Br_2]$	
Bond lengths (Å)			
Zn−N1	2.0575(13)	Cd−N1	2.302(3)
Zn−N2	2.1101(14)	Cd−N2	2.314(3)
Zn−Cl1	2.2332(5)	Cd−Br1	2.5397(6)
Zn−Cl2	2.2103(5)	Cd−Br2	2.5195(6)
N1−C5	1.2845(19)	N1−C5	1.289(5)
C6−C7	1.523(2)	C6−C7	1.519(5)
Bond angles (°)			
N1−Zn1−N2	86.17(5)	N1−Cd1−N2	79.38(11)
N2−Zn1−Cl2	109.71(3)	N2−Cd1−Br2	114.66(8)
N2−Zn1−Cl1	109.81(3)	N2−Cd1−Br1	106.76(8)
N1−Zn1−Cl2	119.21(4)	N1−Cd1−Br2	120.24(8)
N1−Zn1−Cl1	107.41(4)	N1−Cd1−Br1	110.01(8)
Cl2−Zn1−Cl1	119.442(19)	Br2−Cd1−Br1	118.65(3)

whereas a perfect trigonal pyramidal structure generates a THC_{DA} index = 0) and tetracoordinate geometric parameter FCGP,[43] which represents faces as the sum of the angles involved in each polytopal face of the tetracoordinate structure, also provide useful information regarding the tetrahedral geometries of studied complexes.

The $M-N_{imine}$ (2.0575(13)−2.302(3)) Å and $M-N_{amine}$ (2.1101(14)−2.314(3)) Å bond lengths of the synthesized M(II) complexes agreed well with the M−N structural parameters of the studied complexes.[44,45] $M-N_{amine}$ was slightly longer than $M-N_{imine}$ owing to the differences in the hybridization of nitrogen atoms. In addition, the M−Cl and M−Br bond lengths lie within the expected range.[46] The N(1)=C(5) bond distances of 1.2845(19) Å in $[Zn(DE)Cl_2]$ and 1.289(5) Å in $[Cd(DE)Br_2]$ agreed with the accepted C=N double bonds. The C(6)−C(7) bond distances were 1.523(2) Å $[Zn(DE)Cl_2]$ and 1.519(5) Å $[Cd(DE)Br_2]$, demonstrating the lack of delocalized π-electrons. The bond length of $M-N_{amine}$ was larger by about 0.21 Å in $[Cd(DE)Br_2]$ compared to $[Zn(DE)Cl_2]$ owing to the variances in the size of the coordinated metal ions. Additionally, the sulfur of the thiophene moiety did not form a formal bond with the metal center as persistent with our previously reported complexes.[46b]

$N_{imine}-M-N_{amine}$ angles were observed to be smaller compared to $X_{terminal}-M-X_{terminal}$ (X = Cl or Br) angles around the central metal ion in $[Zn(DE)Cl_2]$ and $[Cd(DE)Br_2]$ (Table 2). This represents a structural attribute of $[LMX_2]$-type complexes forming a distorted tetrahedral geometry;[8a] here, L represents the bidentate ligand attached to the metal center and

https://doi.org/10.1021/acsomega.2c08266
ACS Omega 2023, 8, 17620−17633

Table 3. Four-Coordinate Geometry Indices[41] for Zn(II) and Cd(II) Complexes and Illustrative Parameters for Similar Complexes from the Literature

complexes	geometry	τ_4	$THC_{DA}/100$	FCGP/100	reference
square planar (D_{4h})	square planar	0.000	−1.43	−0.400	41
trigonal pyramidal (C_{3v})	trigonal pyramidal	0.850	0.000	1.00	41
$[\mathbf{Zn(DE)Cl_2}]$	tetrahedral	0.861	0.493	0.406	this work
$[\mathbf{Zn(DE)Br_2}]$	tetrahedral	0.859	0.351	0.490	this work
$[\mathbf{Zn(L\text{-}b)_2Cl_2}]^a$	tetrahedral	0.885	0.432	0.452	37b
$[\mathbf{Pd(L\text{-}b)_2Cl_2}]^b$	square planar	0.0626	−1.34	−0.265	37b
$[\mathbf{Zn(L_C)Cl_2}]^b$	tetrahedral	0.887	0.370	0.422	48
$[\mathbf{Pd(L_D)Cl_2}]^c$	tetrahedral	0.870	0.337	0.415	48
$[\mathbf{Zn(L_C)Cl_2}]^d$	square planar	0.0754	−1.31	−0.243	37b
tetrahedral (T_d)	tetrahedral	1.00	1.00	0.000	41

[a] **L-b** = 4-methoxy-*N*-methyl-*N*-(pyridin-2-ylmethyl)aniline.[37b] [b] $\mathbf{L_C}$ = *N*-cyclohexyl-1-(pyridin-2-yl)methanimine.[48] [c] $\mathbf{L_D}$ = 2,6-diethyl-*N*-(pyridin-2-ylmethylene)aniline.[48] [d] $\mathbf{L_C}$ = 4-nitro-*N*-((pyridin-2-yl)methylene)aniline.[37b]

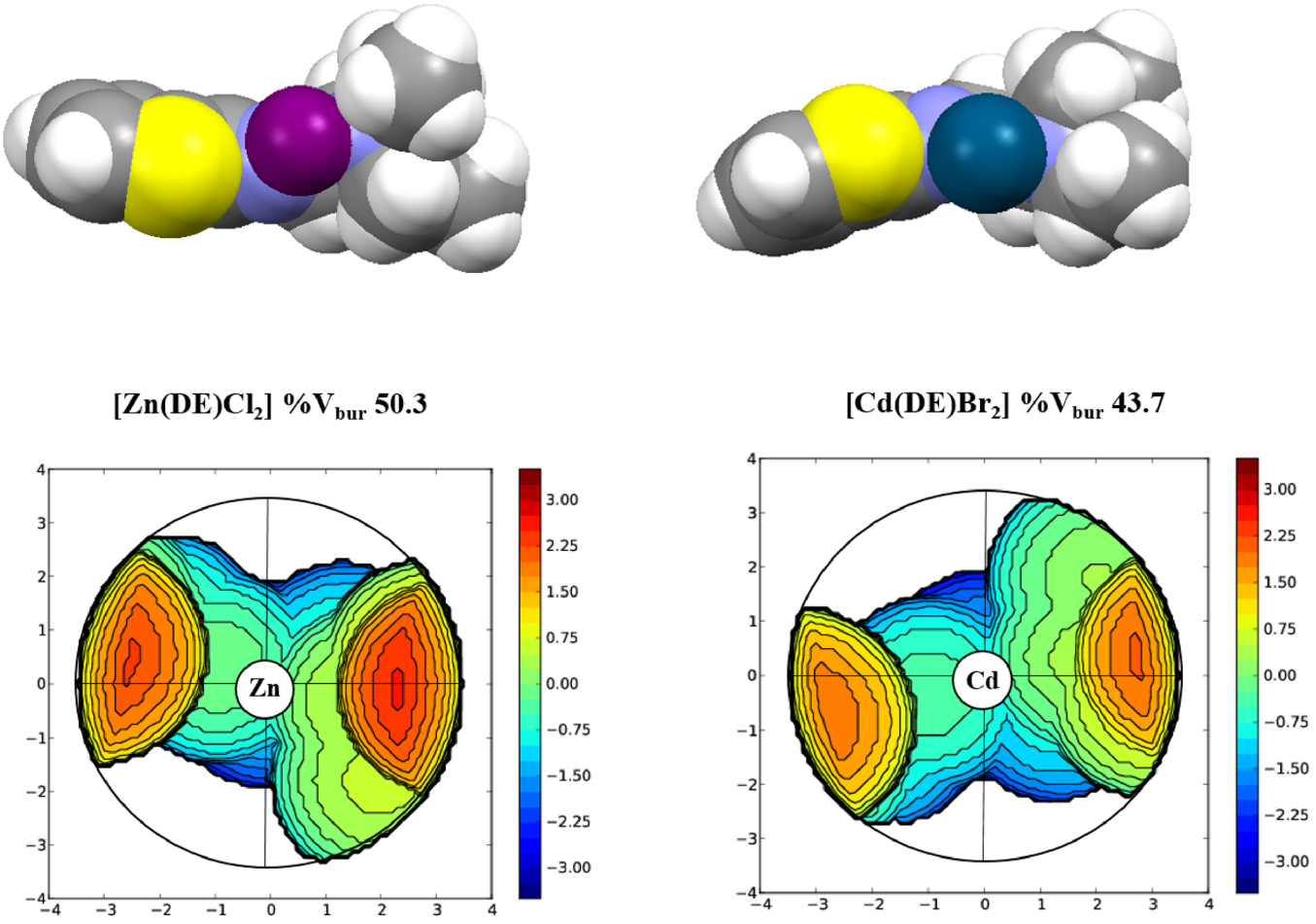

Figure 5. Topographic maps and space filling models of $[\mathbf{Zn(DE)Cl_2}]$ and $[\mathbf{Cd(DE)Br_2}]$ complexes.

X represents a halide. It is evident from X-ray data that the $N_{imine}-M-N_{amine}$ angles lie in an accepted range, i.e., 79.38(11)−86.17(5)°.[46] The plane angle between the thiophene moiety and the five-membered ring N2−C7−C6−N1−Zn1 in $[\mathbf{Zn(DE)Cl_2}]$ was 31.15°, whereas the plane angle between the thiophene moiety and the five-membered ring N2−C7−C6−N1−Cd1 in $[\mathbf{Cd(DE)Br_2}]$ was 43.69°. The buried volumes were calculated using the SambVca 2.1 program,[47] and the steric encumbrance due to the ligand framework around the M(II) (M = Zn and Cd) center was computed by comparing the topographic maps of the studied M(II) complexes (Figure 5). The metal center variation can influence the properties of the M(II) complexes.

3.3. Biological Activities. The characteristics of the metals are of utmost relevance to the biological interactions and toxicity of the complexes; therefore, researchers strive for the development of more effective, target-specific metal-based drugs with minimal toxicity. In addition, steric, electronic, and chelate effects also contribute to the enhanced potency of antimicrobial agents.[49] Cu(II)- and Zn(II)-based complexes are interesting in this regard because these metal ions are biocompatible and contribute to many important biological processes.[49a,50] Zn(II)

https://doi.org/10.1021/acsomega.2c08266
ACS Omega 2023, 8, 17620−17633

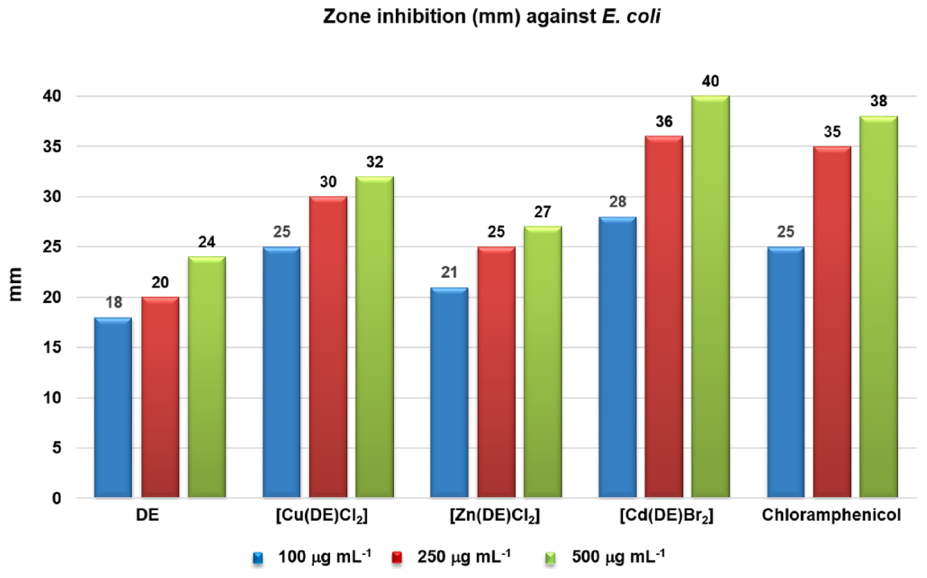

Figure 6. Antibacterial activities of **DE** and its corresponding M(II) complexes against *E. coli*.

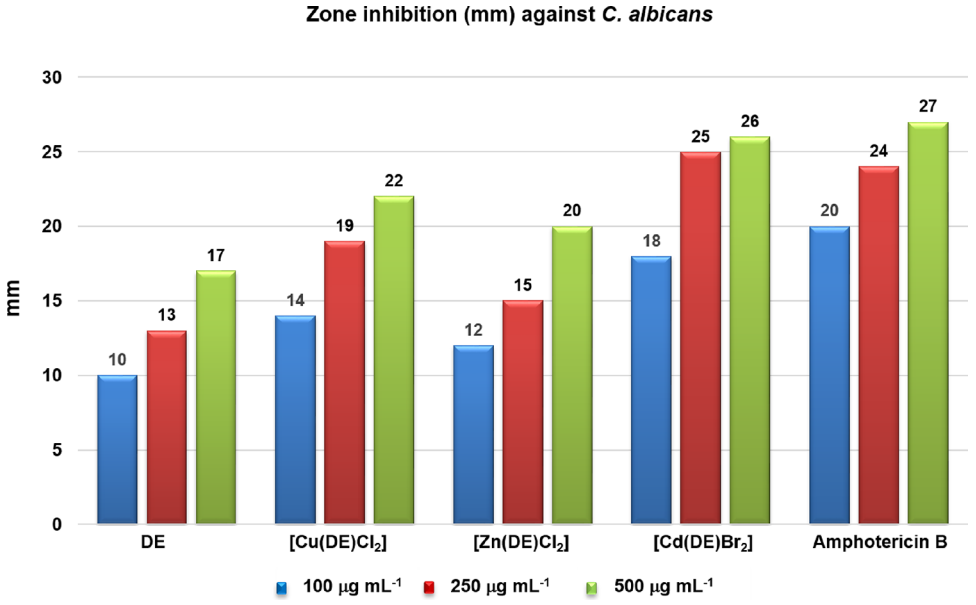

Figure 7. Antifungal activities of **DE** and its M(II) complexes against *C. albicans* at three different concentrations.

represents an essential ion in certain metalloenzymes, whereas Cd is a toxic element present in the environment due to human activities. It rapidly localized intracellularly, especially in the liver, binding to metallo-thionein to form a complex that is slowly transferred to the bloodstream to be deposited in the kidneys. However, recent studies have demonstrated a wide range of pharmacological properties of cadmium complexes with sulfur-derived ligands.[51]

3.3.1. Antibacterial Activities. The antibacterial potencies of the **DE** and its M(II) complexes, $[\mathbf{M(DE)X_2}]$, were tested against two Gram-negative bacteria, *E. coli* and *P. aeruginosa*, and one Gram-positive bacterium, *S. aureus*. The zone of inhibition (diameter in mm) was used to compare the antibacterial activity with that of the standard drug chloramphenicol. The representative antibacterial results, summarized in Table S1, revealed that all the complexes exhibited significant antibacterial activity against the studied bacterial strains since many heavy metals are toxic to microbes as they kill microbes by binding to intracellular proteins and inactivating them. For instance, several coordination compounds exhibited a prominent inhibitory profile. However, the coordination of metal has a pronounced effect on the antibacterial activity of the ligand as well as the metal salts alone. As shown in Table S3, the metal salts have shown lower bactericidal potential and resulted in an enhanced inhibitory profile upon chelation to **DE**. Marked activity of the Cd(II) complex $[\mathbf{Cd(DE)Br_2}]$ was observed among all the studied complexes, with MIC = 10 μg mL^{-1} against *E. coli* (Table S2). This increasing activity of M(II) complexes compared to that of free ligands could also be explained by the chelation theory, and chelation results in a greater decrease in metal ion polarity resulting from the overlap of the ligand orbital and partial sharing of the positive charge of the metal ion with donor groups. Furthermore, the delocalization of π-electrons over the chelate ring promotes the lipid membrane permeation to these complexes and might result in the deterioration of the metal-binding sites in the enzymes of microorganisms.[52] The

https://doi.org/10.1021/acsomega.2c08266
ACS Omega 2023, 8, 17620−17633

complexes were highly active against the Gram-positive bacterium *S. aureus* at 500 and 250 $\mu g\ mL^{-1}$, which were superior to the standard drug chloramphenicol. (Table S2). The reason for such discrepancies in the activities of various strains of bacteria might be due to the difference in the complexity of the cell wall structure of these bacterial strains; therefore, lipo-solubility is an important criterion for controlling microbial growth. The characteristics of the metal ions coordinated to the ligand framework, including the metal ion size and coordination geometry, may play a role in such differences in microbial activities, chelation, and lipophilicity.[52a,53] For instance, Zn(II) and Cd(II), with identical ligand frameworks and geometries but different metal ion sizes and buried volumes, exhibited different antibacterial activities (Figure 6). The same was evident from a recent study by the Demissie group, where the Cu(II) complexes of 2-((2-hydroxyethyl)amino)quinoline-3-carbaldehyde showed higher antibacterial potential than the Zn(II) complexes with the same ligand.[54]

3.3.2. Antifungal Activities. The studied ligand **DE** and its M(II) complexes, $[\mathbf{M(DE)X_2}]$, were tested *in vitro* for their antifungal activities in different concentrations against *C. albicans*. All the screened compounds exhibited significant inhibitory potential against *C. albicans*. It was clear from the data that the activities of the synthesized complexes increased with increasing concentrations of the solutions. Results showed that the $[\mathbf{Cd(DE)Br_2}]$ complex exhibited higher antifungal activity. The order of antifungal activity of the tested compounds at all three concentrations was $[\mathbf{Cd(DE)Br_2}] > [\mathbf{Cu(DE)Cl_2}] > [\mathbf{Zn(DE)Cl_2}] >$ **DE** (Figure 7). The Cd(II) and Cu(II) complexes exhibited higher antifungal activity than the standard. Notably, these complexes might be adsorbed on the cell wall of microorganisms and could also disturb the respiration process of the cell, thus blocking the synthesis of proteins, which restricts the further growth of microorganisms.[53,54]

3.3.3. Antileishmanial Activities. Leishmaniasis is one of the deadliest diseases after malaria that is transmitted *via* sand fly bite, and it affects approximately 1.5 million people per annum. Protozoan parasites of the genus Leishmania can manifest visceral and cutaneous forms of infection in humans.[55] Classical antiparasitic drugs become less effective with the emergence of drug resistance in parasites. Additionally, long-term usage of these leishmanicidal drugs renders them less effective. The inadequate acquaintance with the mechanistic action makes it difficult to overcome these adverse properties.[1,56] Recently, several studies on metal complexes having enhanced leishmanial potential are reported.[57] However, there is still a desire for selective complexes with sulfur-bearing moieties to be preferred because of their similarities to natural products with promising activities against parasites causing leishmaniasis.[33b] Herein, we also tested our studied ligand and M(II) complexes, $[\mathbf{M(DE)X_2}]$, against *L. major* for their leishmanicidal potential.

It is evident from data summarized in Table 4 that the leishmanicidal potential of the studied complexes was superior to amphotericin B. It is a known fact that the ligation of the ligand framework can be enhanced with complexation to transition metals. The metal complexes, $[\mathbf{M(DE)X_2}]$, exhibited greater inhibition profiles than the Schiff base ligand (**DE**) and metal salts alone (Table 4). It is evident that metals inhibit pathogenic growth. In comparison to our studied complexes, we run control experiments using $CuCl_2{\cdot}2H_2O$, $ZnCl_2$, and $CdBr_2{\cdot}4H_2O$ metal salts and found that metal salts without ligand architecture do not show significant inhibition of *L. major* under provided experimental protocols. The order of antileishmanial

Table 4. Antileishmanial Activities of DE and Its M(II) Complexes against *L. major*

S. No	compounds	$IC_{50} \pm SEM^a$ (μM)
1	$CuCl_2{\cdot}2H_2O$	2.7 ± 0.11
2	$ZnCl_2$	5.8 ± 0.07
3	$CdBr_2{\cdot}4H_2O$	1.8 ± 0.01
4	**DE**	2.9 ± 0.01
5	$[\mathbf{Cu(DE)Cl_2}]$	0.54 ± 0.08
6	$[\mathbf{Zn(DE)Cl_2}]$	0.7 ± 0.01
7	$[\mathbf{Cd(DE)Br_2}]$	0.40 ± 0.05
8	amphotericin B	0.58 ± 1.09

[a]SEM = standard error mean (experiment run in triplicate).

inhibition at 100 $\mu g\ mL^{-1}$ for studied complexes was $[\mathbf{Cd(DE)Br_2}] > [\mathbf{Cu(DE)Cl_2}] > [\mathbf{Zn(DE)Cl_2}] >$ **DE** (Table 4). Compared to the Zn(II) complex supported with the *N*-(2-methoxyphenyl)acetamide ligand that exhibited antileishmanial potential (IC_{50} value = 0.78 ± 0.31 μM), our metal complexes, $[\mathbf{M(DE)X_2}]$, showed higher activities.[39] The excellent inhibition profiles of the complexes, $[\mathbf{M(DE)X_2}]$, reported in our study might contribute to the designing of effective metal-derived agents for the treatment of infectious diseases.

3.4. Molecular Docking. Molecular docking is used for identification of various bonding interactions between the docking compound and bioreceptor. This method identifies compounds with greater and lesser affinity for a given receptor. This helps to verify the chemical and geometric interactions of molecules with the receptor active site. In this context, the ligand (**DE**) and its M(II) complexes, $[\mathbf{M(DE)X_2}]$, were theoretically investigated as potent inhibitors of the pathogenic proteins of the studied microbes. The ligand interactions in the active site of receptors and least binding affinity values validated the results.

Figure 8 highlights the major interactions of the studied complexes in the active pocket of receptor protein with amino acid residues of *E. coli*. It is evident that **DE** in the protein receptor active site with the residues Asn46 and Glu50 formed two hydrogen bonding interactions. $[\mathbf{Cu(DE)Cl_2}]$ showed one hydrogen bonding interaction with residue Glu50 having a binding energy around −14.76 kcal mol^{-1} (Table 5). $[\mathbf{Zn(DE)Cl_2}]$ also exhibited hydrogen bonding interaction with the residue Glu50, while $[\mathbf{Cd(DE)Br_2}]$ formed two bonding interactions, i.e., hydrogen bonding with the residues Ile78 and Glu50 with −16.73 kcal mol^{-1} binding energy (Table 5). In the case of *P. aeruginosa*, $[\mathbf{Cu(DE)Cl_2}]$ binds in the active site with residue Ser49 forming one hydrogen bonding interaction and one arene−cation interaction (Figure S14b). $[\mathbf{Zn(DE)Cl_2}]$ formed two bonding interactions with the residues Ser49 and Leu20 (Figure S14c), while $[\mathbf{Cd(DE)Br_2}]$ formed one bonding interaction with residue Lys52 having −17.89 kcal mol^{-1} binding energy (Figure S14d). In the case of *S. aureus*, **DE** with the residues Gly103 and Asp84 formed two hydrogen bonding interactions (Figure S15a), $[\mathbf{Cu(DE)Cl_2}]$ with the residue Gly91 formed one hydrogen bonding interaction (Figure S15b), and $[\mathbf{Zn(DE)Cl_2}]$ with residues Gly103 and Gln27 formed two hydrogen bonding interactions (Figure S15c). $[\mathbf{Cd(DE)Br_2}]$ with the residues Pro29 and Gly103 formed two hydrogen bonding interactions having −12.55 kcal mol^{-1} binding energy (Figure S15d).

The interactions of the M(II) complexes and ligand (**DE**) with *C. albicans* are shown in (Figure S16a−d). **DE** with the residues Leu139 and Cys470 formed two hydrogen bonding interactions. $[\mathbf{Cu(DE)Cl_2}]$ with the residue Ile304 formed a

https://doi.org/10.1021/acsomega.2c08266
ACS Omega 2023, 8, 17620−17633

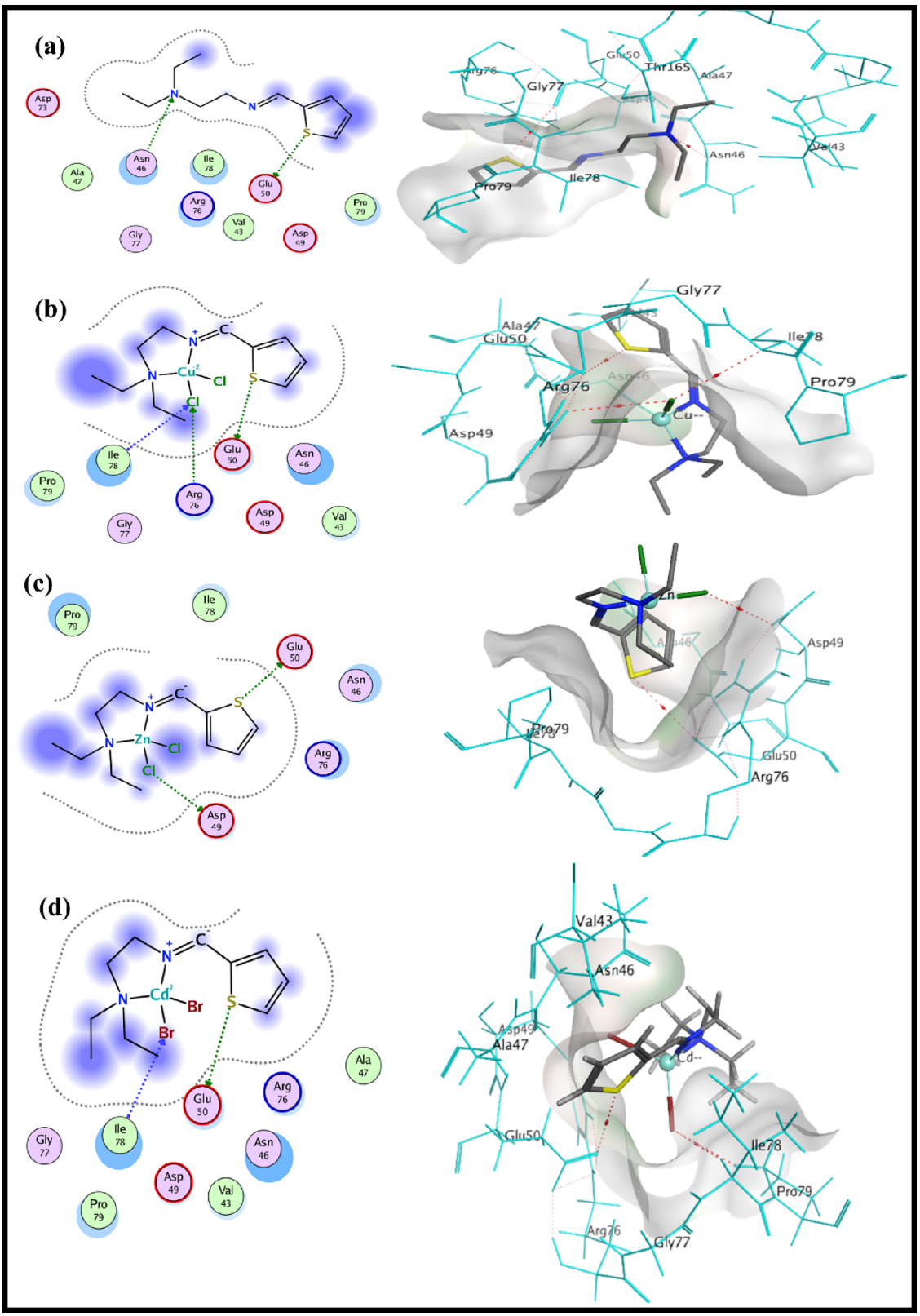

Figure 8. Pictorial description of **DE** (2-D (a) and 3-D (b)); [**Cu(DE)Cl$_2$**] (2-D (a) and 3-D (b)); [**Zn(DE)Cl$_2$**] (2-D (a) and 3-D (b)); [**Cd(DE)Br$_2$**] (2-D (a) and 3-D (b)) representing the interactions with amino acid residues in the active pocket of receptor protein of *E. coli*.

hydrogen bonding with the complex and one arene−cation interaction, whereas [**Zn(DE)Cl$_2$**] also with the residue Phe126 formed one hydrogen bonding interaction. [**Cd(DE)Br$_2$**] with the residue Tyr132 formed one hydrogen bonding interaction and one arene−cation interaction with residue Ile304 with −13.11 kcal mol^{-1} binding energy (Table 5). The interactions of the synthesized ligand and M(II) complexes with *L. major* are shown in Figure S17a−d. **DE** formed one hydrogen bonding

https://doi.org/10.1021/acsomega.2c08266
ACS Omega 2023, 8, 17620−17633

Table 5. Binding Free Energies (ΔG) in kcal mol^{-1} of DE and Its Corresponding M(II) Complexes with Different Targets Obtained Using MOE 2014

S. No	compounds	*E. coli*	*P. aeruginosa*	*S. aureus*	*C. albicans*	*L. major*
1	**DE**	−10.34	−11.34	−10.13	−09.00	−11.34
2	$[Cu(DE)Cl_2]$	−14.76	−12.78	−11.76	−10.89	−15.56
3	$[Zn(DE)Cl_2]$	−15.22	−16.79	−16.33	−17.33	−15.38
4	$[Cd(DE)Br_2]$	−16.73	−17.89	−12.55	−13.11	−12.56

with the residue Ala365 and one $\pi-\pi$ interaction with the residue Tyr198. $[Cd(DE)Br_2]$ formed two hydrogen bonding interactions with residues Tyr198 and Met333 along with one arene−cation interaction with residue Lys60.

4. CONCLUSIONS

In the present study, M(II) complexes, $[M(DE)X_2]$, supported by the thiophene-derived Schiff base ligand **DE**, were synthesized. Spectro-analytical techniques were used for structural characterization of **DE** and its corresponding M(II) complexes. X-ray structural analysis of $[Zn(DE)Cl_2]$ and $[Cd(DE)Br_2]$ showed that the M(II) atom was coordinated *via* two nitrogen atoms of the bidentate ligand, demonstrating a distorted tetrahedral geometry. The efficacy of the synthesized complexes was studied for their antibacterial properties against *E. coli*, *S. aureus*, and *P. aeruginosa*. In addition, antifungal and antileishmanial properties against *C. albicans* and *L. major* were determined, which were further validated through molecular docking studies. It was observed that molecular docking inhibition of selected pathogenic proteins was carried out from each species used in the study as all the pathogenic proteins are essential for pathogens' survival and virology. The results obtained were promising, exhibiting maximum interactions and good binding energies. The $[Cd(DE)Br_2]$ complex can act as a better agent for controlling pathogenic growth compared to its analogs Cu(II) and Zn(II) complexes. The present study revealed the effectiveness of the studied complexes, which could contribute to drug design and show effective results in further *in vivo* experiments and pharmacological assays.

■ ASSOCIATED CONTENT

Supporting Information

The Supporting Information is available free of charge at https://pubs.acs.org/doi/10.1021/acsomega.2c08266.

Crystallographic data for $[Cd(DE)Br_2]$ (CIF)

Crystallographic data for $[Zn(DE)Cl_2]$ (CIF)

^{1}H NMR, ^{13}C NMR, FTIR, and EA for DE and corresponding $[M(DE)X_2]$ complexes (PDF)

■ AUTHOR INFORMATION

Corresponding Authors

Saira Nayab − *Department of Chemistry, Shaheed Benazir Bhutto University (SBBU), Sheringal Upper Dir 18050 Khyber Pakhtunkhwa, Islamic Republic of Pakistan; Department of Chemistry and Green-Nano Materials Research Center, Kyungpook National University, Daegu 41566, Republic of Korea;* orcid.org/0000-0002-9014-1602; Email: drnayab@sbbu.edu.pk

Hyosun Lee − *Department of Chemistry and Green-Nano Materials Research Center, Kyungpook National University, Daegu 41566, Republic of Korea;* orcid.org/0000-0002-0107-3100; Email: hyosunlee@knu.ac.kr

Authors

Aftab Alam − *Department of Chemistry, Shaheed Benazir Bhutto University (SBBU), Sheringal Upper Dir 18050 Khyber Pakhtunkhwa, Islamic Republic of Pakistan*

Nasir Ahmad − *Department of Chemistry, Islamia College University Peshawar, Peshawar 25000 Khyber Pakhtunkhwa, Islamic Republic of Pakistan*

Sher Wali Khan − *Department of Chemistry, Shaheed Benazir Bhutto University (SBBU), Sheringal Upper Dir 18050 Khyber Pakhtunkhwa, Islamic Republic of Pakistan*

Waliullah Khan − *Department of Chemistry, Abdul Wali Khan University, Mardan 23200, Islamic Republic of Pakistan*

Dilawar Farhan Shams − *Department of Environmental Sciences, Abdul Wali Khan University, Mardan 23200, Islamic Republic of Pakistan*

Muhammad Ishaq Ali Shah − *Department of Chemistry, Abdul Wali Khan University, Mardan 23200, Islamic Republic of Pakistan;* orcid.org/0009-0000-3153-7554

Muhammad Ateeq − *Department of Chemistry, Abdul Wali Khan University, Mardan 23200, Islamic Republic of Pakistan*

Said Karim Shah − *Department of Physics, Abdul Wali Khan University, Mardan 23200, Islamic Republic of Pakistan;* orcid.org/0000-0003-0942-2464

Complete contact information is available at: https://pubs.acs.org/10.1021/acsomega.2c08266

Author Contributions

S.N.: conceptualization, supervision-lead, writing the original draft; A.A.: methodology and formal analysis; N.A.: molecular docking studies; S.W.K.: supporting; W.K.: biological studies; D.F.S.: supporting; M.I.A.S.: supporting; M.A.: supporting; S.K.S.: supporting; H.L.: validation, review, and editing.

Notes

The authors declare no competing financial interest.

■ ACKNOWLEDGMENTS

The research presented here was supported by the National Research Program for Universities (NRPU) Grant No. 6840-KP (Higher Education Commission (HEC), Islamabad, Islamic Republic of Pakistan). Additionally, the X-ray crystallography data was obtained with PLS-II 2D-SMC beamline and was supported by MSIP and POSTECH, Republic of Korea.

■ REFERENCES

(1) Catalano, A.; Sinicropi, M. S.; Iacopetta, D.; Ceramella, J.; Mariconda, A.; Rosano, C.; Scali, E.; Saturnino, C.; Longo, P. A review on the advancements in the field of metal complexes with Schiff bases as antiproliferative agents. *Appl. Sci.* **2021**, *11*, 6027.

(2) (a) Pervaiz, M.; Sadiq, S.; Sadiq, A.; Younas, U.; Ashraf, A.; Saeed, Z.; Zuber, M.; Adnan, A. Azo-Schiff base derivatives of transition metal complexes as antimicrobial agents. *Coord. Chem. Rev.* **2021**, *447*, No. 214128. (b) Mohan, C.; Kumar, V.; Kumari, N.; Kumari, S.; Yadav, J.; Gandass, T.; Yadav, S. Synthesis, characterization and antibacterial

activity of semicarbazide based Schiff bases and their Pb(II), Zr(IV) and U(VI) complexes. *Adv. J. Chem., Sect. B* **2020**, *2*, 187−196.
(3) Malik, M. A.; Dar, O. A.; Gull, P.; Wani, M. Y.; Hashmi, A. A. Heterocyclic Schiff base transition metal complexes in antimicrobial and anticancer chemotherapy. *MedChemComm* **2018**, *9*, 409−436.
(4) Bharti, S. K.; Singh, S. K. Metal based drugs: current use and future potential. *Pharm. Lett.* **2009**, *1*, 39−51.
(5) Selvaganapathy, M.; Pravin, N.; Muniyandi, V.; Nazeer, M.; Raman, N. Exploring the photochemosensitivity by novel cysteine-based mixed ligand complexes. *J. Photochem. Photobiol., B* **2016**, *157*, 77−88.
(6) Cozzi, P. G. Metal−Salen Schiff base complexes in catalysis: practical aspects. *Chem. Soc. Rev.* **2004**, *33*, 410−421.
(7) (a) Nithya, P.; Simpson, J.; Govindarajan, S. Syntheses, structural diversity and thermal behavior of first row transition metal complexes containing potential multidentate ligands based on 2, 6-diacetylpyridine and benzyl carbazate. *Polyhedron* **2018**, *141*, 5−16. (b) Iacopetta, D. Special Issue on "Anticancer Drugs Activity and Underlying Mechanisms". *Appl. Sci.* **2021**, *11*, 8169. (c) Kaya, S.; Erkan, S.; Karakaş, D. Computational investigation of molecular structures, spectroscopic properties and antitumor-antibacterial activities of some Schiff bases. *Spectrochim. Acta, Part A* **2021**, *244*, No. 118829. (d) Vijayan, T.; Kim, J.; Azam, M.; Al-Resayes, S. I.; Stalin, A.; Kannan, B. S.; Jayamani, A.; Ayyakannu, A.; Nallathambi, S. Influence of co-ligand on the biological properties of Schiff base metal complexes: Synthesis, characterization, cytotoxicity, and antimicrobial studies. *Appl. Organomet. Chem.* **2022**, *36*, No. e6542.
(8) (a) Lee, J.; Kim, D.; Lee, H.; Nayab, S.; Han, J. H. Effect of initiator on the catalytic performance of zinc(II) complexes supported by aminomethylquinoline and aminomethylpyridine derived ligands in stereoselective ring opening polymerization of *rac*-lactide. *Polyhedron* **2022**, *216*, No. 115696. (b) Kim, K.; Nayab, S.; Jeong, A. R.; Cho, Y.; Yeo, H.; Lee, H. Vinyl-Addition Polymerizations of Norbornene and Methyl Methacrylate by the Palladium(II) Complexes Ligated by 2-Iminomethylquinoline and 2-Iminomethylpyridine Derivatives. *Inorg. Chim. Acta* **2022**, *539*, No. 121025.
(9) (a) Ceyhan, G.; Köse, M.; McKee, V.; Uruş, S.; Gölcü, A.; Tümer, M. Tetradentate Schiff base ligands and their complexes: synthesis, structural characterization, thermal, electrochemical and alkane oxidation. *Spectrochim. Acta, Part A* **2012**, *95*, 382−398. (b) Salih, K. S. M.; Shraim, A. M.; Al-Mhini, S. R.; Al-Soufi, R. E.; Warad, I. New tetradentate Schiff base Cu(II) complexes: synthesis, physicochemical, chromotropism, fluorescence, thermal, and selective catalytic oxidation. *Emergent Mater.* **2021**, *4*, 423−434.
(10) (a) Segura, J. L.; Mancheño, M. J.; Zamora, F. Covalent organic frameworks based on Schiff-base chemistry: synthesis, properties and potential applications. *Chem. Soc. Rev.* **2016**, *45*, 5635−5671. (b) More, M. S.; Joshi, P. G.; Mishra, Y. K.; Khanna, P. K. Metal complexes driven from Schiff bases and semicarbazones for biomedical and allied applications: a review. *Mater. Today Chem.* **2019**, *14*, No. 100195. (c) Chaudhary, N. K.; Mishra, P. Metal complexes of a novel Schiff base based on penicillin: characterization, molecular modeling, and antibacterial activity study. *Bioinorg. Chem. Appl.* **2017**, *2017*, 1. (d) Chen, Z.; Brookhart, M. Exploring ethylene/polar vinyl monomer copolymerizations using Ni and Pd α-diimine catalysts. *Acc. Chem. Res.* **2018**, *51*, 1831−1839.
(11) (a) Singh, H. L.; Varshney, A. Synthetic, structural, and biochemical studies of organotin(IV) with Schiff bases having nitrogen and sulphur donor ligands. *Bioinorg. Chem. Appl.* **2006**, *2006*, 23245. (b) Ejidike, I.; Ajibade, P. Ruthenium(III) complexes of heterocyclic tridentate (ONN) Schiff base: Synthesis, characterization and its biological properties as an antiradical and antiproliferative agent. *Int. J. Mol. Sci.* **2016**, *17*, 60. (c) Mengesha, D. N.; Kim, H. Electronic structure modulation of multi-walled carbon nanotubes using azo dye for inducing non-radical reaction: Effect of graphitic nitrogen and structural defect. *Chemosphere* **2022**, *307*, No. 136023. (d) Hossain, A. M. S.; Méndez-Arriaga, J. M.; Xia, C.; Xie, J.; Gómez-Ruiz, S. Metal complexes with ONS donor Schiff bases. A review. *Polyhedron* **2022**, No. 115692. (e) Afroz, L.; Moinuddin Khan, M. H.; Vagdevi, H. M.; Pari, M.; Mohammed Shafeeualla, R.; Mussuvir Pasha, K. M. Investigation on Co(II), Ni(II), Cu(II) and Zn(II) complexes derived from novel N′-(3-hydroxybenzoyl) thiophene-2-carbohydrazide: structural characterization, electrochemical detection of biomolecules, molecular docking and biological evaluation. *Emergent Mater.* **2022**, *5*, 1133−1155.
(12) (a) Sudha, D.; Vairam, S.; Sarathbabu, S.; Senthil Kumar, N.; Sivasamy, R.; Jone Kirubavathy, S. 2-Methylimidazolium pyridine-2,5-dicarboxylato zinc(II) dihydrate: Synthesis, characterization, DNA interaction, anti-microbial, anti-oxidant and anti-breast cancer studies. *J. Coord. Chem.* **2021**, *74*, 2701−2719. (b) Yasmeen, S.; Sumrra, S. H.; Akram, M. S.; Chohan, Z. H. Antimicrobial metal-based thiophene derived compounds. *J. Enzyme Inhib. Med. Chem.* **2017**, *32*, 106−112. (c) Shah, R.; Verma, P. K. Synthesis of thiophene derivatives and their anti-microbial, antioxidant, anticorrosion and anticancer activity. *BMC Chem.* **2019**, *13*, 1−13. (d) Puthran, D.; Poojary, B.; Purushotham, N.; Harikrishna, N.; Nayak, S. G.; Kamat, V. Synthesis of novel Schiff bases using 2-Amino-5-(3-fluoro-4-methoxyphenyl) thiophene-3-carbonitrile and 1,3-Disubstituted pyrazole-4-carboxaldehydes derivatives and their antimicrobial activity. *Heliyon* **2019**, *5*, No. e02233.
(13) Panneerselvam, P.; Nair, R. R.; Vijayalakshmi, G.; Subramanian, E. H.; Sridhar, S. K. Synthesis of Schiff bases of 4-(4-aminophenyl)-morpholine as potential antimicrobial agents. *Eur. J. Med. Chem.* **2005**, *40*, 225−229.
(14) Aljahdali, M. S.; El-Sherif, A. A.; Hilal, R. H.; Abdel-Karim, A. T. Mixed bivalent transition metal complexes of 1,10-phenanthroline and 2-aminomethylthiophenyl-4-bromosalicylaldehyde Schiff base: Spectroscopic, molecular modeling and biological activities. *Eur. J. Chem.* **2013**, *4*, 370−378.
(15) Hassan, F. S.; Fayez, M.; Abdalla, N. Coordination behavior and biological activity of some transition metal complexes with 2-acetyl and 2-formyl-3-amino-1, 4-naphthoquinone ligands. *Open J. Inorg. Non-Met. Mater.* **2020**, *10*, 54.
(16) Shin, J. W.; Eom, K.; Moon, D. BL2D-SMC, the supramolecular crystallography beamline at the Pohang Light Source II, Korea. *J. Synchrotron Radiat.* **2016**, *23*, 369−373.
(17) (a) Otwinowski, Z.; Borek, D.; Majewski, W.; Minor, W. Multiparametric scaling of diffraction intensities. *Acta Crystallogr., Sect. A: Found. Crystallogr.* **2003**, *59*, 228−234. (b) Otwinowski, Z.; Minor, W. [20] Processing of X-ray diffraction data collected in oscillation mode. *Methods Enzymol.* **1997**, *276*, 307−326.
(18) Sheldrick, G., *SADABS—Bruker Nonius Scaling and Absorption Correction*; Bruker AXS. Inc.: Madison, WI, USA 2012.
(19) Sheldrick, G. M. SHELXT−Integrated space-group and crystal-structure determination. *Acta Crystallogr., Sect. A: Found. Adv.* **2015**, *A71*, 3−8.
(20) Sheldrick, G. M. Crystal structure refinement with SHELXL. *Acta Crystallogr., Sect. C: Struct. Chem.* **2015**, *C71*, 3−8.
(21) Kondori, T.; Akbarzadeh-T, N.; Fazli, M.; Mir, B.; Dušek, M.; Eigner, V. A novel schiff base ligand and its copper complex: Synthesis, characterization, X-ray crystal structure and biological evaluation. *J. Mol. Struct.* **2021**, *1226*, No. 129395.
(22) Balouiri, M.; Sadiki, M.; Ibnsouda, S. K. Methods for in vitro evaluating antimicrobial activity: A review. *J. Pharm. Anal.* **2016**, *6*, 71−79.
(23) Habtemariam, S. *In vitro* antileishmanial effects of antibacterial diterpenes from two Ethiopian Premna species: P. schimperi and P. oligotricha. *BMC Pharmacol.* **2003**, *3*, 6.
(24) Kompis, I. M.; Islam, K.; Then, R. L. DNA and RNA synthesis: antifolates. *Chem. Rev.* **2005**, *105*, 593−620.
(25) Hawser, S.; Lociuro, S.; Islam, K. Dihydrofolate reductase inhibitors as antibacterial agents. *Biochem. Pharmacol.* **2006**, *71*, 941−948.
(26) Schnell, J. R.; Dyson, H. J.; Wright, P. E. Structure, dynamics, and catalytic function of dihydrofolate reductase. *Annu. Rev. Biophys. Biomol. Struct.* **2004**, *33*, 119−140.
(27) (a) Lafitte, D.; Lamour, V.; Tsvetkov, P. O.; Makarov, A. A.; Klich, M.; Deprez, P.; Moras, D.; Briand, C.; Gilli, R. DNA gyrase interaction with coumarin-based inhibitors: the role of the hydrox-

https://doi.org/10.1021/acsomega.2c08266
ACS Omega 2023, 8, 17620−17633

ybenzoate isopentenyl moiety and the 5 '-methyl group of the noviose. *Biochemistry* **2002**, *41*, 7217−7223. (b) Moynié, L.; Hope, A. G.; Finzel, K.; Schmidberger, J.; Leckie, S. M.; Schneider, G.; Burkart, M. D.; Smith, A. D.; Gray, D. W.; Naismith, J. H. A substrate mimic allows high-throughput assay of the FabA protein and consequently the identification of a novel inhibitor of *Pseudomonas aeruginosa* FabA. *J. Mol. Biol.* **2016**, *428*, 108−120. (c) Oefner, C.; Parisi, S.; Schulz, H.; Lociuro, S.; Dale, G. E. Inhibitory properties and X-ray crystallographic study of the binding of AR-101, AR-102 and iclaprim in ternary complexes with NADPH and dihydrofolate reductase from *Staphylococcus aureus*. *Acta Crystallogr., Sect. D: Biol. Crystallogr.* **2009**, *65*, 751−757. (d) Hargrove, T. Y.; Friggeri, L.; Wawrzak, Z.; Qi, A.; Hoekstra, W. J.; Schotzinger, R. J.; York, J. D.; Guengerich, F. P.; Lepesheva, G. I. Structural analyses of *Candida albicans* sterol 14α-demethylase complexed with azole drugs address the molecular basis of azole-mediated inhibition of fungal sterol biosynthesis. *J. Biol. Chem.* **2017**, *292*, 6728−6743.

(28) (a) Krauth-Siegel, R. L.; Comini, M. A. Redox control in trypanosomatids, parasitic protozoa with trypanothione-based thiol metabolism. *Biochim. Biophys. Acta, Gen. Subj.* **2008**, *1780*, 1236−1248. (b) Linares, G.; Ravaschino, E.; Rodriguez, J. Progresses in the field of drug design to combat tropical protozoan parasitic diseases. *Curr. Med. Chem.* **2006**, *13*, 335−360.

(29) (a) Dumas, C.; Ouellette, M.; Tovar, J.; Cunningham, M. L.; Fairlamb, A. H.; Tamar, S.; Olivier, M.; Papadopoulou, B. Disruption of the trypanothione reductase gene of Leishmania decreases its ability to survive oxidative stress in macrophages. *EMBO J.* **1997**, *16*, 2590−2598. (b) Fairlamb, A. H.; Blackburn, P.; Ulrich, P.; Chait, B. T.; Cerami, A. Trypanothione: a novel bis (glutathionyl) spermidine cofactor for glutathione reductase in trypanosomatids. *Science* **1985**, *227*, 1485−1487. (c) Flohe, L.; Hecht, H. J.; Steinert, P. Glutathione and trypanothione in parasitic hydroperoxide metabolism. *Free Radical Biol. Med.* **1999**, *27*, 966−984. (d) Krieger, S.; Schwarz, W.; Ariyanayagam, M. R.; Fairlamb, A. H.; Krauth-Siegel, R. L.; Clayton, C. Trypanosomes lacking trypanothione reductase are avirulent and show increased sensitivity to oxidative stress. *Mol. Microbiol.* **2000**, *35*, 542−552. (e) Tovar, J.; Wilkinson, S.; Mottram, J. C.; Fairlamb, A. H. Evidence that trypanothione reductase is an essential enzyme in Leishmania by targeted replacement of the tryA gene locus. *Mol. Microbiol.* **1998**, *29*, 653−660.

(30) Kumar, Y. N.; Kumar, P. S.; Sowjenya, G.; Rao, V. K.; Yeswanth, S.; Prasad, U. V.; Pradeepkiran, J. A.; Sarma, P.; Bhaskar, M. Comparison and correlation of binding mode of ATP in the kinase domains of Hexokinase family. *Bioinformation* **2012**, *8*, 543.

(31) Labute, P. The generalized Born/volume integral implicit solvent model: estimation of the free energy of hydration using London dispersion instead of atomic surface area. *J. Comput. Chem.* **2008**, *29*, 1693−1698.

(32) Mishra, R.; Jha, K.; Kumar, S.; Tomer, I. Synthesis, properties and biological activity of thiophene: A review. *Pharma Chem.* **2011**, *3*, 38−54.

(33) (a) Raman, N.; Jeyamurugan, R.; Senthilkumar, R.; Rajkapoor, B.; Franzblau, S. G. In vivo and in vitro evaluation of highly specific thiolate carrier group copper(II) and zinc(II) complexes on Ehrlich ascites carcinoma tumor model. *Eur. J. Med. Chem.* **2010**, *45*, 5438−5451. (b) Hashem, H. E.; Nath, A.; Kumer, A. Synthesis, molecular docking, molecular dynamic, quantum calculation, and antibacterial activity of new Schiff base-metal complexes. *J. Mol. Struct.* **2022**, *1250*, No. 131915.

(34) Nakamoto, K., *Infrared and Raman spectra of inorganic and coordination compounds, part B: applications in coordination, organometallic, and bioinorganic chemistry*; John Wiley & Sons: 2009.

(35) Lee, J.; Melchakova, I.; Nayab, S.; Kim, K.; Ko, Y. H.; Yoon, M.; Avramov, P.; Lee, H. Synthesis and Characterization of Zinc(II), Cadmium(II), and Palladium(II) Complexes with the Thiophene-Derived Schiff Base Ligand. *ACS Omega* **2023**, *8*, 6016−6029.

(36) Kim, K.; Nayab, S.; Cho, Y.; Jung, H.; Yeo, H.; Lee, H.; Lee, S.-H. Catalytic performance of tridentate versus bidentate Co(II) complexes supported by Schiff base ligands in vinyl addition polymerization of norbornene. *RSC Adv.* **2022**, *12*, 35896−35904.

(37) (a) Lee, J.; Kim, K.; Lee, H.; Nayab, S. Cobalt(II) complexes supported by iminomethylpyridine derived ligands: Synthesis, characterization and catalytic application towards methyl methacrylate and *rac*-lactide polymerisations. *Polyhedron* **2021**, *196*, No. 115003. (b) Park, S.; Lee, J. K.; Lee, H.; Nayab, S.; Shin, J. W. Zinc(II), palladium(II) and cadmium(II) complexes containing 4-methoxy-*N*-(pyridin-2-ylmethylene) aniline derivatives: Synthesis, characterization and methyl methacrylate polymerization. *Appl. Organomet. Chem.* **2019**, *33*, No. e4797.

(38) Vairalakshmi, M.; Princess, R.; Rani, B. K.; Raja, S. J. Synthesis, structural elucidation, catalytic, antibacterial and antioxidant activity of thiophene derived mixed ligand metal complexes. *J. Chil. Chem. Soc.* **2018**, *63*, 3844−3849.

(39) Sultana, K.; Zaib, S.; Khan, I.; Shahid, K.; Simpson, J.; Iqbal, J. Exploiting the potential of aryl acetamide derived Zn(II) complexes in medicinal chemistry: synthesis, structural analysis, assessment of biological profile and molecular docking studies. *New J. Chem.* **2016**, *40*, 7084−7094.

(40) John, L.; Joseyphus, R. S.; Joe, I. H. Biomedical application studies of Schiff base metal complexes containing pyridine moiety: molecular docking and a DFT approach. *SN Appl. Sci.* **2020**, *2*, 500.

(41) Yang, L.; Powell, D. R.; Houser, R. P. Structural variation in copper(I) complexes with pyridylmethylamide ligands: structural analysis with a new four-coordinate geometry index, τ_4. *Dalton Trans.* **2007**, 955−964.

(42) Höpfl, H. The tetrahedral character of the boron atom newly defined—a useful tool to evaluate the N→ B bond. *J. Organomet. Chem.* **1999**, *581*, 129−149.

(43) Hutchison, A. R.; Mitra, A.; Atwood, D. A. The four coordinate geometric parameter: A new quantification of geometry for four coordinate aluminum and gallium. *Main Group Chem.* **2005**, *4*, 187−200.

(44) Tyagi, P.; Chandra, S.; Saraswat, B. S. Ni(II) and Zn(II) complexes of 2-((thiophen-2-ylmethylene) amino) benzamide: Synthesis, spectroscopic characterization, thermal, DFT and anticancer activities. *Spectrochim. Acta, Part A* **2015**, *134*, 200−209.

(45) Sun, Y.-X. Dichloro [*N*,*N*-dimethyl-*N*'-(pyridin-2-ylmethylidene) ethane-1, 2-diamine] zinc (II). *Acta Crystallogr., Sect. E: Struct. Rep. Online* **2005**, *61*, m373−m374.

(46) (a) Lee, J.; Lee, H.; Nayab, S.; Yoon, K. B. Synthesis, characterization and polymerisation studies of cadmium(II) complexes containing *N*,*N*′,*X*-tridentate X-substituted (X= N, O) 2-iminomethylpyridines. *Polyhedron* **2019**, *158*, 432−440. (b) Kwon, K. S.; Nayab, S.; Lee, H.; Jeong, J. H. Synthesis and structural characterisation of zinc complexes bearing furanylmethyl and thiophenylmethyl derivatives of (*R*,*R*)-1,2-diaminocyclohexanes for stereoselective polymerisation of poly (*rac*-lactide). *Polyhedron* **2014**, *77*, 32−38.

(47) Falivene, L.; Credendino, R.; Poater, A.; Petta, A.; Serra, L.; Oliva, R.; Scarano, V.; Cavallo, L. SambVca 2. A web tool for analyzing catalytic pockets with topographic steric maps. *Organometallics* **2016**, *35*, 2286−2293.

(48) Heo, J.; Lee, H.; Nayab, S. Polymerizations of methyl methacrylate and *rac*-lactide by zinc(II) precatalyst containing N-substituted 2-iminomethylpyridine and 2-iminomethylquinoline. *J. Coord. Chem.* **2017**, *70*, 3837−3858.

(49) (a) Osredkar, J.; Sustar, N. Copper and zinc, biological role and significance of copper/zinc imbalance. *J. Clin. Toxicol.* **2011**, *3*, 3. (b) Uba, A.; Ladan, M. M.; Adamu, U. A.; Magaji, B.; Ibrahim, M. N.; Sani, M. M. Synthesis, Characterization and Antibacterial Assay of Some Schiff base Metal(II) Complexes. *Adv. Res.* **2020**, *21*, 28−34. (c) Abdel-Rahman, L. H.; Abu-Dief, A. M.; Shehata, M. R.; Atlam, F. M.; Abdel-Mawgoud, A. A. H. Some new Ag(I), VO(II) and Pd(II) chelates incorporating tridentate imine ligand: Design, synthesis, structure elucidation, density functional theory calculations for DNA interaction, antimicrobial and anticancer activities and molecular docking studies. *Appl. Organomet. Chem.* **2019**, *33*, No. e4699. (d) Aljohani, F. S.; Abu-Dief, A. M.; El-Khatib, R. M.; Al-

https://doi.org/10.1021/acsomega.2c08266
ACS Omega 2023, 8, 17620−17633

Abdulkarim, H. A.; Alharbi, A.; Mahran, A.; Khalifa, M. E.; El-Metwaly, N. M. Structural inspection for novel Pd(II), VO(II), Zn(II) and Cr(III)-azomethine metal chelates: DNA interaction, biological screening and theoretical treatments. *J. Mol. Struct.* **2021**, *1246*, No. 131139.

(50) Drewry, J. A.; Gunning, P. T. Recent advances in biosensory and medicinal therapeutic applications of zinc (II) and copper (II) coordination complexes. *Coord. Chem. Rev.* **2011**, *255*, 459−472.

(51) (a) López-Torres, E.; Mendiola, M. A.; Rodríguez-Procopio, J.; Sevilla, M. T.; Colacio, E.; Moreno, J. M.; Sobrados, I. Synthesis and characterisation of zinc, cadmium and mercury complexes of benzilbisthiosemicarbazone. Structure of cadmium derivative. *Inorg. Chim. Acta* **2001**, *323*, 130−138. (b) Alomar, K.; Landreau, A.; Kempf, M.; Khan, M. A.; Allain, M.; Bouet, G. Synthesis, crystal structure, characterization of zinc(II), cadmium(II) complexes with 3-thiophene aldehyde thiosemicarbazone (3TTSCH). Biological activities of 3TTSCH and its complexes. *J. Inorg. Biochem.* **2010**, *104*, 397−404. (c) Palm, M.; Fransson, A.; Hultén, J.; Búcaro Stenman, K.; Allouche, A.; Chiang, O. E.; Constandse, M. L.; van Dijk, K. J.; Icli, S.; Klimesova, B.; Korhonen, E.; Martínez-Crespo, G.; Meggers, D.; Naydenova, M.; Polychronopoulou, M. A.; Schuntermann, D. B.; Unal, H.; Wasylkowska, A.; Farewell, A. The Effect of Heavy Metals on Conjugation Efficiency of an F-Plasmid in *Escherichia coli*. *Antibiotics* **2022**, *11*, 1123.

(52) (a) Murukan, B.; Mohanan, K. Synthesis, characterization and antibacterial properties of some trivalent metal complexes with [(2-hydroxy-1-naphthaldehyde)-3-isatin]-bishydrazone. *J. Enzyme Inhib. Med. Chem.* **2007**, *22*, 65−70. (b) Chohan, Z. H.; Pervez, H.; Khan, K. M.; Supuran, C. T. Organometallic-based antibacterial and antifungal compounds: transition metal complexes of 1,1′-diacetylferrocene-derived thiocarbohydrazone, carbohydrazone, thiosemicarbazone and semicarbazone. *J. Enzyme Inhib. Med. Chem.* **2005**, *20*, 81−89. (c) Franklin, T. J. Uptake of tetracycline by membrane preparations from *Escherichia coli*. *Biochem. J.* **1971**, *123*, 267−273. (d) Pasdar, H.; Foroughifar, N.; Saghavaz, B. H. Synthesis, characterization and antibacterial activity of Co(II), Ni(II), Mn(II), Cu(II) and Zn(II) complexes with 2-amino-7, 7-dimethyl-5-oxo-4-chlorobenzen 5, 6,7, 8-tetra hydro-4H-chromene-3-carbonitrile. *Heath biotechnol. biopharma.* **2017**, *1*, 64−71.

(53) Srivastva, A. N.; Singh, N. P.; Shriwastaw, C. K. *In vitro* antibacterial and antifungal activities of binuclear transition metal complexes of ONNO Schiff base and 5-methyl-2, 6-pyrimidine-dione and their spectroscopic validation. *Arabian J. Chem.* **2016**, *9*, 48−61.

(54) Damena, T.; Alem, M. B.; Zeleke, D.; Desalegn, T.; Eswaramoorthy, R.; Demissie, T. B. Novel zinc(II) and copper(II) complexes of 2-((2-hydroxyethyl) amino) quinoline-3-carbaldehyde for antibacterial and antioxidant activities: A combined experimental, DFT, and docking studies. *ACS Omega* **2022**, *7*, 26336−26352.

(55) (a) Scorza, B.; Carvalho, E.; Wilson, M. Cutaneous manifestations of human and murine leishmaniasis. *Int. J. Mol. Sci.* **2017**, *18*, 1296. (b) Severino, P.; Santana, W.; Lisboa, E. S.; Santos, V. L. d.; Lima, E. T. d. S.; Cardoso, J. C.; Albuquerque-Junior, R. L. d.; Naveros, B. C.; Santini, A.; Souto, E. B. Cutaneous/Mucocutaneous Leishmaniasis Treatment for Wound Healing: Classical versus New Treatment Approaches. *Microbiol. Res.* **2022**, *13*, 836−852.

(56) Condé, C. A.; De Almeida, M. V.; Da Silva, G. d. S.; Sodré, M. B. P. d. A.; Rodrigues, J. C. F.; Navarro, M. Synthesis, characterization and antileishmanial activity of copper(II) and zinc(II) complexes with diamine ligands. *Transition Met. Chem.* **2022**, *47*, 147−156.

(57) (a) Tahghighi, A. Importance of metal complexes for development of potential leishmanicidal agents. *J. Organomet. Chem.* **2014**, *770*, 51−60. (b) Braga, S. S. Ruthenium Complexes, an Emerging Class of Leishmanicidal Drug Candidates. *Appl. Biosci.* **2022**, *1*, 129−142.

https://doi.org/10.1021/acsomega.2c08266
ACS Omega 2023, 8, 17620−17633